JACS
JOURNAL OF THE AMERICAN CHEMICAL SOCIETY

Communication

pubs.acs.org/JACS

High-Efficiency Photoelectrocatalytic Hydrogen Generation Enabled by Palladium Quantum Dots-Sensitized TiO_2 Nanotube Arrays

Meidan Ye,[†] Jiaojiao Gong,[†] Yuekun Lai,[†] Changjian Lin,*[,†] and Zhiqun Lin*[,‡]

[†]State Key Laboratory of Physical Chemistry of Solid Surfaces, and Department of Chemistry, College of Chemistry and Chemical Engineering, Xiamen University, Xiamen 361005, China

[‡]School of Materials Science and Engineering, Georgia Institute of Technology, Atlanta, Georgia 30332, United States

Supporting Information

ABSTRACT: TiO_2 nanotube arrays (TNTAs) sensitized by palladium quantum dots (Pd QDs) exhibit highly efficient photoelectrocatalytic hydrogen generation. Vertically oriented TNTAs were prepared by a three-step electrochemical anodization. Subsequently, Pd QDs with uniform size and narrow size distribution were formed on TiO_2 nanotubes by a modified hydrothermal reaction (i.e., yielding nanocomposites of Pd QDs deposited on TNTAs, Pd@TNTAs). By exploiting Pd@TNTA nanocomposites as both photoanode and cathode, a substantially increased photon-to-current conversion efficiency of nearly 100% at λ = 330 nm and a greatly promoted photocatalytic hydrogen production rate of 592 μmol·h^{-1}·cm^{-2} under 320 mW·cm^{-2} irradiation were achieved. The synergy between nanotubular structures of TiO_2 and uniformly dispersed Pd QDs on TiO_2 facilitated the charge transfer of photoinduced electrons from TiO_2 nanotubes to Pd QDs and the high activity of Pd QDs catalytic center, thereby leading to high-efficiency photoelectrocatalytic hydrogen generation.

Photoelectrocatalytic water splitting is widely recognized as one of the most promising routes to large-scale production of hydrogen as a potential fuel for renewable energy.[1] Among the various catalysts, the noble metal palladium has attracted much attention as one of the most versatile candidates utilized in hydrogen-relevant reactions.[2] In particular, Pd immobilized on diverse supports, including carbon, silicates, amorphous or mesoporous silica, and porous biomaterials or polymers, exhibits remarkable performance in organic transformations and especially coupling and hydrogenation reactions.[3−6] One-dimensional highly ordered TiO_2 nanotube arrays (TNTAs) fabricated by electrochemical anodization have been demonstrated as a promising photoanode for use in photocatalytic water splitting and solar energy conversion with markedly improved efficiency.[7−13] Modified TNTAs were found to possess attractive activities for photoelectrocatalytic water splitting.[14,15] However, due to the fast recombination of photogenerated electrons and holes, it remains a major challenge to successfully capitalize on TNTAs for photocatalytic applications.

It is well known that the catalytic properties of composites of transition metal particles and supporting materials depend heavily upon the metal particle size, dispersion, composition, etc.[16,17] In this context, it is of high importance to prepare such composites with uniform dispersion, tunable particle size, and narrow size distribution to promote their catalytic activities.[18] Catalysts made of Pd nanoparticles supported on TNTAs (i.e., Pd@TNTA nanocomposites) are expected to enhance TiO_2 photocatalysis for hydrogen generation; this can be ascribed to their prominent charge-transfer and separation properties and stability against photocorrosion.[19] The latter contrasts sharply with most of semiconductors, such as CdS, which cause photocorrosion and are not suitable for water splitting.[19] As the Fermi level of Pd is lower than that of TiO_2, photoexcited electrons can be readily transferred from TiO_2 to Pd particles deposited on the surface of TiO_2, thereby significantly reducing the possibility of electron−hole recombination and leading to efficient charge separation and greater photocatalytic reactions.

To date, several elegant studies have centered on the preparation of noble metal particles supported on TiO_2, including physical vapor deposition (PVD) and particle precipitation (PP) of Pd nanoparticles on TiO_2 nanotubes,[20] and *in situ* loading of noble metals on TiO_2 through a redox reaction between the reductive titanium(III) oxide support and metal salt precursors.[21] This *in situ* approach was relatively simple but exhibited low control over the metal particle size and dispersion. While the PVD and PP methods showed better potential to overcome these problems, they suffered from some inherent drawbacks, such as high cost and complicated operation. Clearly, in order to further enhance photoelectrocatalytic reactivity, there is a need to develop more effective techniques to yield high-quality Pd@TNTAs with sufficiently small Pd quantum dots (QDs, down to a few nanometers) homogeneously dispersed on geometrically ordered TNTAs.

Herein, we report a *facile* synthetic strategy for crafting TNTAs sensitized by Pd QDs (Pd@TNTAs) with superior performance in hydrogen production via photoelectrocatalytic water splitting. Highly ordered TNTAs were fabricated by a three-step electrochemical anodization of Ti foil.[14] Subsequently, Pd QDs were deposited on crystalline TiO_2 nanotubes via a modified hydrothermal process in which the initial concentration of poly(vinylpyrrolidone) (PVP) in the reaction solution, reaction time, and temperature were found to have profound influences on the size of Pd QDs and the amount of Pd loading. In particular, Pd@TNTA nanocomposites with the same amount of Pd loading but different sizes of Pd QDs, or vice versa (i.e., nanocomposites with the same size of Pd QDs but different Pd

Received: August 6, 2012
Published: September 10, 2012

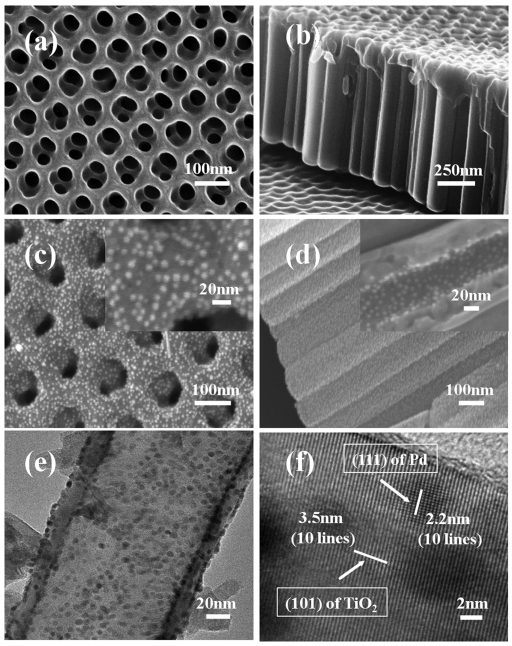

Figure 1. (a) Top and (b) cross-sectional SEM images of TiO_2 nanotube arrays obtained from a three-step electrochemical anodization. SEM images of Pd QDs deposited on TNTAs: (c) top view at low and high (inset) magnifications, and (d) cross-sectional view (a high magnification of a broken tube is shown in the inset). TEM images of TiO_2 nanotubes with Pd QDs deposited: (e) Pd QDs were uniformly dispersed on the nanotube, and (f) a HRTEM image in which a few Pd QDs deposited on the nanotube are clearly evident.

loading), can be *controllably* prepared. Photoelectrochemical (PEC) measurements were performed in a three-electrode PEC cell. Notably, compared to 370 μmol·h^{-1}·cm^{-2} when pure TNTAs were used, by capitalizing on Pd@TNTAs as both photoanode and cathode, a significantly enhanced photocatalytic hydrogen generation rate of 592 μmol·h^{-1}·cm^{-2} under 320 mW·cm^{-2} irradiation resulted, with an incident photon-to-current conversion efficiency (IPCE) of nearly 100% at λ = 330 nm.

Figure 1a shows a typical SEM image of TNTAs in which highly ordered, compact, one-dimensional architechture is clearly evident. The nanotube arrays were crack-free, with an average tube diameter of 80 nm and a wall thickness of 30 nm. The nanotubes were very smooth, with an average tube length of only 1.2 μm, obtained after a three-step anodization (Figure 1b; experimental details in SI). It is noteworthy that these ordered TNTAs possessed large porosity (Figure 1a), which is highly favorable for uniform deposition of Pd QDs. The amorphous TiO_2 nanotubes were transformed into anatase form after thermal annealing at 450 °C in air for 2 h. As evidenced in Figure 1c,d, after hydrothermal reaction of $PdCl_2$ in the presence of anatase TNTAs in the solution of PVP and NaI at 200 °C for 1.5 h (see SI), the Pd QDs obtained were homogeneously dispersed over the entire surface of the nanotubes, both inside (inset in Figure 1d) and outside (Figure 1d and inset in Figure 1c) of the nanotubes. The integrity of nanotubular structures was retained and was not influenced by the hydrothermal processing. The corresponding energy-dispersive X-ray (EDX) analysis (see SI) suggested that the amount of Pd QD deposits was ~2.15 wt%. A representative TEM image of Pd QDs on an individual TiO_2 nanotube (i.e., Pd@TNTA) is shown in Figure 1e, revealing a uniform distribution of Pd QDs on the nanotube with very small particle size of 3.3 ± 0.7 nm (Figure S1). The average lattice spacing of 0.35 nm (marked in the left in Figure 1f) corresponds to the (101) plane of anatase TiO_2,[22] while the lattice spacing of 0.22 nm originates from the (111) plane of metallic Pd.[23]

The elemental composition of Pd@TNTA nanocomposites was analyzed by X-ray photoelectron spectroscopy (XPS, see SI). As shown in Figure S2, the emergence of two fitted peaks of Pd $3d_{5/2}$ at 335.2 and 337.4 eV can be assigned to Pd^0 and Pd^{2+}, respectively.[24] The presence of Pd^0 indicated that part of the Pd was loaded on the surface of TiO_2 as QDs, while the presence of Pd^{2+} implied the existence of PdO, possibly from surface oxidation of Pd metal.[25] In addition, the XRD pattern of Pd@TNTAs (Figure S3) clearly shows the diffractions of TiO_2 nanotubes and Ti foil, with a diffraction peak of Pd (200) at 46.5°. That the peak positions of anatase shifted to lower angles suggested a lattice expansion of TiO_2, as the large Pd^{2+} ions (0.080 nm) might replace Ti^{4+} ions (0.064 nm) in TiO_2 crystals.[24] Thus, the XRD results indicate that Pd exists as Pd QDs and PdO in the system, correlating well with the XPS analysis. Notably, the size of Pd QDs and the amount of Pd loading can be tuned by varying the initial concentration of PVP in the reaction solution, reaction time, and temperature (Figures S4−S6). The amount of Pd QDs loading was extremely crucial to PEC activities (see Figure S7 and discussion in SI).

Figure 2a summarizes the IPCE obtained from the PEC cell (Scheme S1) by employing either pure TNTAs or Pd@TNTAs (Pd% = 2.15 wt%) as photoanode at 0.9 V_{SCE}. The absorption edges of Pd@TNTAs displayed an obvious blue-shift from 350 to 330 nm, which can be attributed to the quantum confinement effect from Pd QDs.[24] It is interesting to note that, by replacing the conventional Pt cathode with Pd@TNTAs as cathode, enhanced IPCE was observed under the same experimental conditions, signifying a more efficient and inexpensive route to photocatalytic hydrogen generation.[2] The maximum IPCE ($IPCE_{max}$) obtained from the PEC cell utilizing Pd@TNTAs as photoanode and cathode (down-triangles in Figure 2a) was ~98.6% at λ = 330 nm; this is in stark contrast to 69.8% at λ = 350 nm when pure TNTA photoanode and Pd@TNTA cathode were used (up-triangles in Figure 2a). On the other hand, the $IPCE_{max}$ obtained with Pd@TNTA photoanode and Pt cathode was roughly 90.6% at λ = 335 nm (circles in Figure 2a), while it was 65.1% at λ = 350 nm with pure TNTA photoanode and Pt cathode (squares in Figure 2a). The photocurrent density measured from highly ordered TNTAs before and after deposition of Pd QDs in 0.5 M KOH in a PCE cell is shown in Figure 2b. Notably, the photocurrent density responded to Pd@TNTA photoanode (down-triangles and circles curves) much more than to TNTA photoanode (up-triangles and square curves) at all applied potentials. Intriguingly, replacing Pt cathode (i.e., square and circle curves) with Pd@TNTAs (i.e., up-triangles and down-triangles curves) yielded an improved performance of the PEC cell. The PEC cell exploiting the Pd@TNTA nanocomposites as both photoanode and cathode exhibited the highest photocurrent density, up to 26.8 mA·cm^{-2} at a potential of 0.9 V (vs SCE) under the same irradiation. It is not surprising that, in line with the IPCE and photocurrent results, the rate of hydrogen generation with Pd@TNTAs employed as both photoanode and cathode for photoelectrocatalytic water splitting reached 592 μmol·h^{-1}·cm^{-2} (i.e., ~2960 μmol/cm^2 generated in 5 h, Figure 2c) in 2 M Na_2CO_3 and 0.5 M ethylene glycol (as sacrificial agent) at bias voltage of −0.3 V (vs SCE) (Scheme S1 and discussion in SI), which was about 1.6 times faster than that of a conventional Pt

dx.doi.org/10.1021/ja307449z | J. Am. Chem. Soc. 2012, 134, 15720−15723

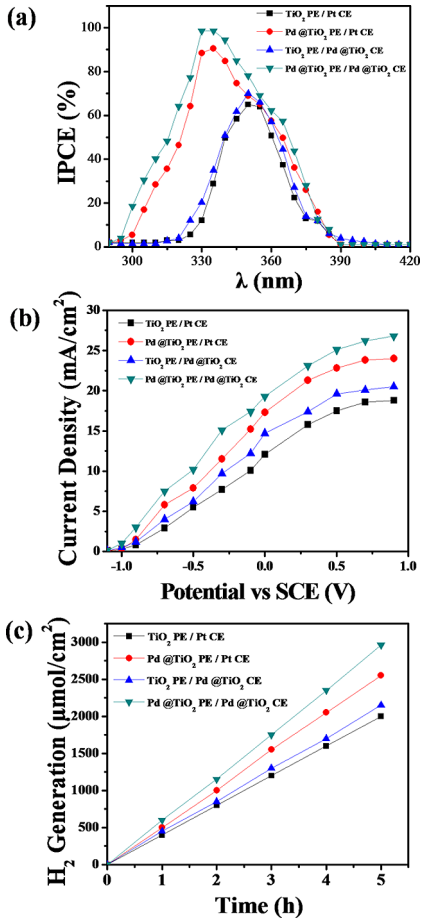

Figure 2. (a) Incident photon-to-current conversion efficiency (IPCE) measured at 0.9 V_{SCE} in 0.5 M KOH. (b) Photocurrent density generated by utilizing TiO_2 nanotubes and Pd@TNTA nanocomposites as photoanodes and Pt foil and Pd@TNTAs nanocomposites as cathodes in 0.5 M KOH in a photoelectrochemical (PEC) cell at a potential range of −1.1 to −0.9 V vs SCE, under 320 mW·cm^{-2} irradiation. (c) Amount of hydrogen generated by capitalizing on TiO_2 nanotubes and Pd@TNTAs nanocomposites as photoanodes and Pt foil and Pd@TNTA nanocomposites as cathodes at −0.3 V_{SCE} in a PEC cell containing a 2 M Na_2CO_3 and 0.5 M ethylene glycol solution under 320 mW·cm^{-2} irradiation. Pd% = 2.15 wt%. PE and CE indicate photoanode electrode and cathode electrode, respectively.

cathode/TiO_2 photoanode pair (1900 μmol/cm^2, Figure 2c). To our knowledge, this unusually high hydrogen generation rate represents a significant improvement as compared to previous work.[14,15] The linear relationship of hydrogen generation as a function of time suggests that the Pd@TNTA nanocomposites were stable during the measurement. In the hydrogen generation experiment, at bias voltage of −0.3 V_{SCE}, the amount of O_2 evolved was only 105 μmol·h^{-1}·cm^{-2}, much lower than expected on the basis of the stoichiometric ratio (i.e., H_2:O_2 = 2:1). This may be attributed to the holes consumed by the addition of electron donor (ethylene glycol) in the electrolyte and the absorbed oxygen on the photocatalyst surface under UV irradiation.

The interfacial properties between the electrode (i.e., TNTAs and Pd@TNTAs) and the electrolyte were scrutinized by electrochemical impedance spectroscopy (EIS) measurements. A semicircle (i.e., the arch in the present study) in the Nyquist plot at high frequency represents the charge-transfer process, while the diameter of the semicircle reflects the charge-transfer

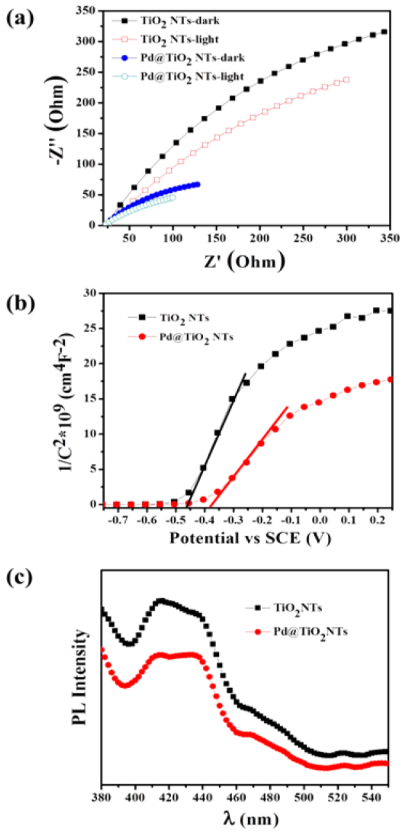

Figure 3. (a) Nyquist plot of electrochemical impedance spectra, (b) Mott−Schottky plots, and (c) photoluminescence (PL) spectra of TNTAs and Pd@TNTAs (Pd% = 2.15 wt%) at room temperature.

resistance (Figure 3a). Clearly, the arches for Pd@TNTAs both in the dark and under 320 mW·cm^{-2} illumination were much smaller than those for TNTAs, implying that decoration with Pd QDs significantly enhanced the electron mobility by reducing the recombination of electron−hole pairs. Moreover, the capacitance measurement was performed on the electrode/electrolyte according to the Mott−Schottky equation,[26,27]

$$\frac{1}{C^2} = \frac{2}{N_D e \varepsilon_0 \varepsilon}\left(E - E_{FB} - \frac{kT}{e}\right) \quad (1)$$

where C is the space charge capacitance in the semiconductor, N_D is the electron carrier density, e is the elemental charge, ε_0 is the permittivity of a vacuum, ε is the relative permittivity of the semiconductor, E is the applied potential, E_{FB} is the flat band potential, T is the temperature, and k is the Boltzmann constant. Figure 3b displays the Mott−Schottky plots of $1/C^2$ as a function of the applied potential, from which the positive slopes (i.e., lines) were observed, suggesting n-type semiconductors. Furthermore, the plots were extrapolated to $1/C^2 = 0$ to estimate the values of E_{FB} (eq 1), giving −0.461 and −0.381 V for TNTAs and Pd@TNTAs, respectively. Notably, compared to TNTAs, a positive shift of E_{FB} in Pd@TNTAs demonstrated a decrease in bending of the band edge, thereby facilitating the electron transfer. In addition, the carrier density N_D can also be calculated from Figure 3b using the following equation:[27]

$$N_D = \frac{2}{e\varepsilon_0\varepsilon}\left(\frac{dE}{d\left(\frac{1}{C^2}\right)}\right) \quad (2)$$

dx.doi.org/10.1021/ja307449z | J. Am. Chem. Soc. 2012, 134, 15720−15723

As $e = 1.6 \times 10^{-19}$ C, $\varepsilon_0 = 8.86 \times 10^{-12}$ F/m, and $\varepsilon = 48$ for anatase TiO_2, the N_D values of TNTAs and Pd@TNTAs were determined to be 3.28×10^{17} and 6.44×10^{17} cm^{-3}, respectively. Consequently, the higher N_D of Pd@TNTAs signified a faster carrier transfer than in TNTAs, and thus an enhanced PEC performance.[27]

We note that the capability of charge separation by Pd QDs can also be verified by analysis of the photoluminescence (PL) spectra as shown in Figure 3c. PL measurements are often employed to study surface processes involving electron−hole recombination of TiO_2. Briefly, after irradiation of the photocatalyst, electron−hole pairs undergo a recombination process, and photons are then emitted, resulting in PL.[28] As shown in Figure 3c, a broad-band emission around 410 nm wavelength (excited at 325 nm) can be attributed to the recombination of photoexcited holes with electrons occupying the singly ionized oxygen vacancies in TiO_2. Therefore, the PL intensity for Pd@TNTAs was decreased as compared to that of TNTAs, indicating a reduced charge carrier recombination.[24]

The markedly enhanced photocatalytic activity for hydrogen production was a direct consequence of synergetic effects of the highly ordered nanotubular TiO_2 matrix and uniformly dispersed Pd QDs (Scheme S2). First, the crystalline nature of TiO_2 together with its nanotubular geometry provided a large surface area for fast and efficient transfer of photogenerated electrons to Pd QDs. Second, it is well known that the photoexcited electrons and holes can easily recombine to decrease the photocatalytic efficiency; in the present study, the Pd QDs, acting as electron sinks, reduced the recombination of electrons and holes and extended their lifetime (lower right panel in Scheme S2), leading to a greatly improved photocurrent and efficiency of H_2 generation.[29] Finally, the Pd QDs loaded on TNTAs played a crucial role as catalytic centers in facilitating water decomposition and hydrogen production.[6,30]

In summary, we have developed a promising and efficient strategy of crafting uniform Pd QDs with very narrow particle size distribution ($D = 3.3 \pm 0.7$ nm) loaded on highly ordered TiO_2 nanotube arrays by capitalizing on a modified hydrothermal reaction. The substantially increased photon-to-current conversion efficiency (nearly 100% at $\lambda = 330$ nm by utilizing Pd@TNTAs as both photoanode and cathode) and notably promoted photocatalytic hydrogen production rate (1.6 times over the conventional counterpart) reflected that the synergy between the nanotubular geometry of TiO_2 and uniformly dispersed Pd QDs facilitated the charge transfer of photoexcited electrons from TiO_2 nanotubes to Pd QDs and the high activity of Pd QD catalytic centers for high-efficiency photoelectrocatalytic hydrogen generation.

■ ASSOCIATED CONTENT

Supporting Information

Experimental methods, FESEM and TEM images of samples prepared for control experiments, XPS and XRD profiles of samples, photocurrent density curve, and device schemes. This material is available free of charge via the Internet at http://pubs.acs.org.

■ AUTHOR INFORMATION

Corresponding Author

cjlin@xmu.edu.cn; zhiqun.lin@mse.gatech.edu

Notes

The authors declare no competing financial interest.

■ ACKNOWLEDGMENTS

C.L. gratefully acknowledges financial support from the National Natural Science Foundation of China (51072170, 21021002), the National Basic Research Program of China (2012CB932900), and Academic New Artist Ministry of Education Doctoral Post Graduate of China (2010). Z.L. gratefully acknowledges the support from Georgia Institute of Technology.

■ REFERENCES

(1) Fujishima, A.; Honda, K. *Nature* **1972**, *238*, 37−38.
(2) Huang, Y.-X.; Liu, X.-W.; Sun, X.-F.; Sheng, G.-P.; Zhang, Y.-Y.; Yan, G.-M.; Wang, S.-G.; Xu, A.-W.; Yu, H.-Q. *Int. J. Hydrogen Energy* **2011**, *36*, 2773−2776.
(3) Erathodiyil, N.; Ooi, S.; Seayad, A. M.; Han, Y.; Lee, S. S.; Ying, J. Y. *Chem.—Eur. J.* **2008**, *14*, 3118−3125.
(4) Gronnow, M. J.; Luque, R.; Macquarrie, D. J.; Clark, J. H. *Green Chem.* **2005**, *7*, 552−557.
(5) Lee, S.-S.; Park, B.-K.; Byeon, S.-H.; Chang, F.; Kim, H. *Chem. Mater.* **2006**, *18*, 5631−5633.
(6) Wang, Y.; Yao, J.; Li, H.; Su, D.; Antonietti, M. *J. Am. Chem. Soc.* **2011**, *133*, 2362−2365.
(7) Wang, J.; Lin, Z. Q. *J. Phys. Chem. C* **2009**, *113*, 4026−4030.
(8) Wang, J.; Zhao, L.; Lin, V. S. Y.; Lin, Z. Q. *J. Mater. Chem.* **2009**, *19*, 3682−3687.
(9) Wang, J.; Lin, Z. Q. *Chem. Mater.* **2010**, *22*, 579−584.
(10) Ye, M.; Xin, X.; Lin, C.; Lin, Z. *Nano Lett.* **2011**, *11*, 3214−3220.
(11) Xin, X.; Wang, J.; Han, W.; Ye, M.; Lin, Z. *Nanoscale* **2012**, *4*, 964−969.
(12) Macak, J. M.; Tsuchiya, H.; Taveira, L.; Aldabergerova, S.; Schmuki, P. *Angew. Chem., Int. Ed.* **2005**, *44*, 7463−7465.
(13) Mor, G. K.; Shankar, K.; Paulose, M.; Varghese, O. K.; Grimes, C. A. *Nano Lett.* **2006**, *6*, 215−218.
(14) Gong, J.; Lai, Y.; Lin, C. *Electrochim. Acta* **2010**, *55*, 4776−4782.
(15) Gong, J.; Lin, C.; Ye, M.; Lai, Y. *Chem. Commun.* **2011**, *47*, 2598−2600.
(16) Chen, M.; Goodman, D. W. *Acc. Chem. Res.* **2006**, *39*, 739−746.
(17) Corma, A.; Serna, P.; García, H. *J. Am. Chem. Soc.* **2007**, *129*, 6358−6359.
(18) Valden, M.; Lai, X.; Goodman, D. W. *Science* **1998**, *281*, 1647−1650.
(19) Ni, M.; Leung, M. K. H.; Leung, D. Y. C.; Sumathy, K. *Renew. Sustain. Energy Rev.* **2007**, *11*, 401−425.
(20) Honciuc, A.; Laurin, M.; Albu, S.; Sobota, M.; Schmuki, P.; Libuda, J. *Langmuir* **2010**, *26*, 14014−14023.
(21) Xie, Y.; Ding, K.; Liu, Z.; Tao, R.; Sun, Z.; Zhang, H.; An, G. *J. Am. Chem. Soc.* **2009**, *131*, 6648−6649.
(22) Mohapatra, S. K.; Misra, M.; Mahajan, V. K.; Raja, K. S. *J. Phys. Chem. C* **2007**, *111*, 8677−8685.
(23) Xiong, Y.; Chen, J.; Wiley, B.; Xia, Y.; Yin, Y.; Li, Z.-Y. *Nano Lett.* **2005**, *5*, 1237−1242.
(24) Chang, Y.; Xu, J.; Zhang, Y.; Ma, S.; Xin, L.; Zhu, L.; Xu, C. *J. Phys. Chem. C* **2009**, *113*, 18761−18767.
(25) Safonova, O. V.; Rumyantseva, M. N.; Kozlov, R. I.; Labeau, M.; Delabouglise, G.; Ryabova, L. I.; Gaskov, A. M. *Mater. Sci. Eng., B* **2000**, *77*, 159−166.
(26) O'Hayre, R.; Nanu, M.; Schoonman, J.; Goossens, A. *J. Phys. Chem. C* **2007**, *111*, 4809−4814.
(27) Zhang, Z.; Yu, Y.; Wang, P. *ACS Appl. Mater. Interfaces* **2012**, *4*, 990−996.
(28) Zhang, N.; Liu, S.; Fu, X.; Xu, Y.-J. *J. Phys. Chem. C* **2011**, *115*, 9136−9145.
(29) Nakao, R.; Rhee, H.; Uozumi, Y. *Org. Lett.* **2004**, *7*, 163−165.
(30) Yamauchi, M.; Abe, R.; Tsukuda, T.; Kato, K.; Takata, M. *J. Am. Chem. Soc.* **2011**, *133*, 1150−1152.